Research Article

Advances in Mechanical Engineering

Advances in Mechanical Engineering
1–8

DOI: 10.1177/1687814015581269
aime.sagepub.com
SAGE

Experimental study of thermophysical properties and nanostructure of self-assembled water/polyalphaolefin nanoemulsion fluids

Jiajun Xu[1], Boualem Hammouda[2], Fangyu Cao[3] and Bao Yang[3]

Abstract

In this study, the nanostructures and thermophysical properties (thermal conductivity, viscosity, and specific heat) of one new type of nanostructured heat transfer fluid, water/polyalphaolefin nanoemulsion fluid, are investigated. The water/polyalphaolefin nanoemulsion fluids are thermodynamically stable containing dispersed water nanodroplets formed by self-assembly. It has been found that the nanostructure inside nanoemulsion fluids may affect their thermophysical properties, especially the phase change heat transfer characteristics. The small-angle neutron scattering technique has been used to help identify the nanostructure inside the water/polyalphaolefin nanoemulsion fluids. By using the 3-region Guinier–Porod model, the fitting curve shows that there is a nonlinear variation of the nanodroplets' size and shape with water's concentration, which also coincides with the trend of its viscosity and specific heat. On the other hand, the thermal conductivity increases linearly with higher volume fraction of water which, however, appears to be insensitive to the nanostructure change. While the water nanodroplets inside can increase the thermal conductivity of the nanoemulsion fluid by 16%, its effective specific heat can be boosted up to 90% when the water nanodroplets undergo liquid–solid phase change.

Keywords

Nanoemulsion fluid, thermophysical properties, self-assembly, small-angle neutron scattering

Date received: 20 November 2014; accepted: 3 February 2015

Academic Editor: Moran Wang

Introduction

Advanced thermal management is a complex and challenging problem widely faced in industrial and military applications.[1–12] Conventional coolants, lubricants, and other heat transfer fluids used in today's thermal management systems typically have relatively poor heat transfer properties. Hence, utilizing the phase change process to increase the heat transfer properties of conventional fluids is another promising direction.[13–16] Recently, the author has proposed a new "nanoemulsion heat transfer fluid" system in which one liquid of lower boiling point is dispersed into another immiscible liquid and formed self-assembled nanodroplets which help improving the fluid thermal properties especially

[1]Department of Mechanical Engineering, University of the District of Columbia, Washington, DC, USA
[2]Center for Neutron Research, National Institute of Standards and Technology (NIST), Gaithersburg, MD, USA
[3]Department of Mechanical Engineering, University of Maryland, College Park, MD, USA

Corresponding author:
Jiajun Xu, Department of Mechanical Engineering, University of the District of Columbia, Washington, DC 20008, USA.
Email: jiajun.xu@udc.edu

its phase change characteristics.[7,12,17–32] The nanoemulsion heat transfer fluids belong to the family of self-assembled colloid system and are thermodynamically stable.

The customization capability of the thermophysical properties—through forming different nanodroplets inside—makes them attractive candidates for emerging heat transfer applications in various industries. For example, the added nanodroplets of higher thermal conductivity can improve the thermal conductivity of the nanoemulsion fluids and transfer heat more effectively.

In this article, the thermophysical characteristics of water/polyalphaolefin (PAO) nanoemulsion fluids—thermal conductivity, viscosity, and specific heat—are investigated experimentally, along with a structure characterization of nanostructures formed inside using small-angle neutron scattering (SANS).

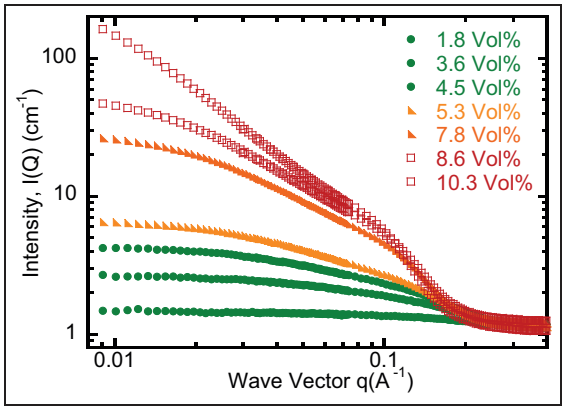

Figure 1. Small-angle neutron scattering curves for water/PAO nanoemulsion fluids: water volume concentration from 1.8% to 10.3% volume fraction. Three different colors represent three different types of scattering curves. The statistical error bars are smaller than the plotting symbols.

Measurement methods

Structure characterization

SANS measurements were carried out for the characterization of the nanostructures. One great advantage of using SANS is that it can be applied to "concentrated" colloidal suspensions (e.g. >1% volume fraction) for the in situ determination of the size of droplets in the nanoemulsion fluids and is better suited than conventional dynamic light scattering.[33–39] In the SANS experiments, samples are prepared using deuterated water (D_2O) to achieve the needed contrast between the droplets and the solvent. SANS measurements were conducted on the NG-3 (30 m) beamline at the NIST Center for Neutron Research (NCNR) in Gaithersburg, MD. Samples are loaded into 2-mm quartz cells and kept at room temperature. Figure 1 shows the SANS data for water volumetric concentration covering 1.8%–3% volume fraction. The scattering intensity I versus the scattering vector

$$q = \frac{4\pi \sin(\theta/2)}{\lambda} \tag{1}$$

where λ is the wavelength of the incident neutrons and θ is the scattering angle. The approximation $q = 2\pi\theta/\lambda$ is used for SANS (due to the small angle θ).

Thermal conductivity measurement

3ω-wire method is used here for the thermal conductivity measurement. The 3ω-wire method is a combination of the 3ω method and the hot-wire method.[23–25,40–46] Similar to the hot-wire method, a metal wire suspended in a liquid acts as both heater and thermometer. A sinusoidal current frequency is passed through the metal wire and generated a heat wave at frequency 2ω. The temperature rise at frequency 2ω in the metal wire can be deduced by the voltage component at frequency 3ω. The thermal conductivity of the liquid, κ, is determined by the slope of the 2ω temperature rise of the metal wire with respect to the frequency ω

$$\kappa = \frac{p}{4\pi l}\left(\frac{\partial T_{2\omega}}{\partial \ln \omega}\right)^{-1} \tag{2}$$

where p is the applied electric power, ω is the frequency of the applied electric current, l is the length of the metal wire, and $T_{2\omega}$ is the amplitude of temperature oscillation at frequency 2ω in the metal wire. One advantage of this 3ω-wire method is that the temperature oscillation can be kept small enough (below 1 K, compared to about 5 K for the hot-wire method) within the test liquid to retain constant liquid properties.

Viscosity measurement

Viscosity is defined by considering the force applied in the course of flow of a fluid, and its dissipation per unit area and velocity gradient is the viscosity

$$F = \mu A \frac{u}{y} \tag{3}$$

where F is the stress force, u is the velocity, y is the separation, A is the area, and μ is the proportionality factor called dynamic viscosity.

The viscosity of a nanoemulsion fluid depends largely on its microstructure, that is, the type of aggregates that are present, on their interactions, and on the

concentration of the system.[20,22,24,41,47–49] Therefore, the viscosity can be used to monitor the structural changes in the nanoemulsion system, and on the other hand, the structural change can also be reflected in the viscosity measured.

Specific heat measurement

A differential scanning calorimeter (DSC) was used to measure a nanoemulsion fluid's specific heat. Usually DSC measurement can be made in two ways: by measuring the electrical power provided to heaters below the pans necessary to maintain the two pans at the same temperature (power compensation) and by measuring the heat flow (differential temperature) as a function of sample temperature (heat flux). The DSC ultimately outputs the differential heat flow (heat/time) between the measured material and the empty reference pan.

The heat capacity may be determined by taking the ratio of heat flow to heating rate. Thus

$$c_p = \frac{q}{\Delta T} \tag{4}$$

where c_p is the material's heat capacity, q is the heat flow through the material over a given time, and ΔT is the change in temperature over that same time.

The specific heats of the pure PAO and water/PAO nanoemulsion fluids are measured using a heat-flux-type DSC (TA-Q100). This is accomplished by comparing the heat flux into a pan containing the sample with the heat flux into an empty pan. In this method, both the measured sample and reference sample are maintained at nearly the same temperature by adjusting heat input to them. The difference in the amount of heat supplied to the sample and the reference is recorded as a function of temperature (or time). In the curve of heat flux versus temperature or versus time, positive or negative peaks correspond to exothermic or endothermic reactions in the sample, respectively. Enthalpies of phase transitions can be calculated by integrating the peak corresponding to a given transition, $\Delta H = c \cdot A$ where A is the area under the peak and c is the calorimetric constant. In order to determine the sample heat capacity, three measurements are usually carried out: for the sample, for the baseline, and for a standard. The baseline is subtracted from the sample measurement to obtain absolute values of the heat flow to the sample. The heat capacity is determined by the heat flow, the temperature rise, and the sample mass.

Experimental results and discussion

Structural change characterization

Figure 1 shows the SANS data for water/PAO nanoemulsion fluids with water volumetric concentration covering 1.8%–10.3% volume fraction.

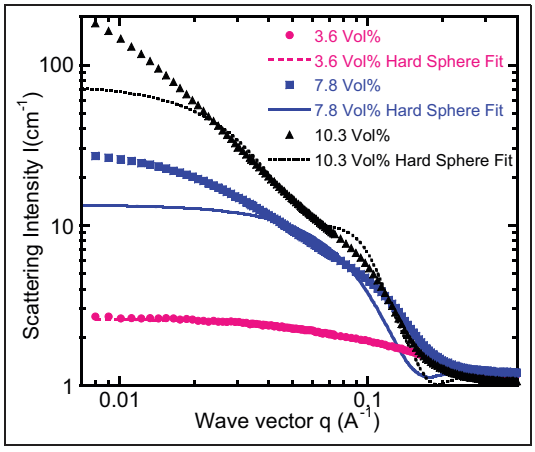

Figure 2. Small-angle neutron scattering curves for water/PAO nanoemulsion fluids (solid symbols) and hard-sphere model curve fittings (colored lines).

It is clear from the SANS data that the neutron scattering data gradually change into three different types of curves with increasing water loading. Based on the shape of the scattering curves, they can be classified into three ranges: the 1.8%–4.5% volume fraction ones with a smooth and gradually increasing scattering intensity for low-q range (less than 0.1 Å); the 5.3%–7.8% volume fraction ones with a sharper increase of q for the high-q range (larger than 0.1 Å) and a flatter intensity curve for low-q (less than 0.03 Å); and for even higher concentrations like 8.6% and 10.3% volume fractions ones tested here, the "hump" for high q is even more obvious and the intensity for low q increases more sharply which gives very obvious three sections of scattering curves. For colloidal systems which do not experience inner structure change, the SANS data can be fitted using one model. However, most colloidal systems including nanoemulsion fluids can undergo inner structure change with change in concentration, temperature, salinity, and so on. Especially for the water/PAO nanoemulsion fluids, the simple correlation length model cannot fit all the SANS curves well for both low and high-q regions as shown in Figure 2.

The hard-sphere model fits well for low water concentrations (i.e. 1.8%–4.5% volume fraction), and nanodroplet radii are found to be 13.2, 25.6, and 96 Å for water loading 1.8%, 3.6%, and 4.5% volume fractions, respectively. For higher water concentration (i.e. 7.8%–10.3% volume fraction), the hard-sphere model does not fit well especially for scattering variable q less than 0.1 Å region, which suggests that those nanodroplets are not simply spherical.

To describe the structure variation inside the water/PAO nanoemulsion fluids more accurately, another fitting model is used to describe the structure change. The 3-region Guinier–Porod empirical model is used to

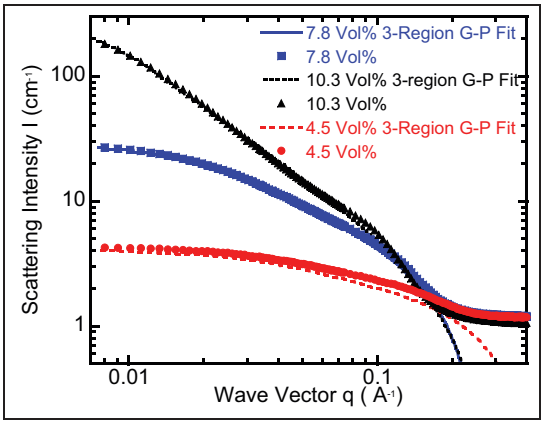

Figure 3. Small-angle neutron scattering curves for water in PAO nanoemulsion fluids (solid symbols) and 3-region Guinier–Porod model curve fittings (colored lines).

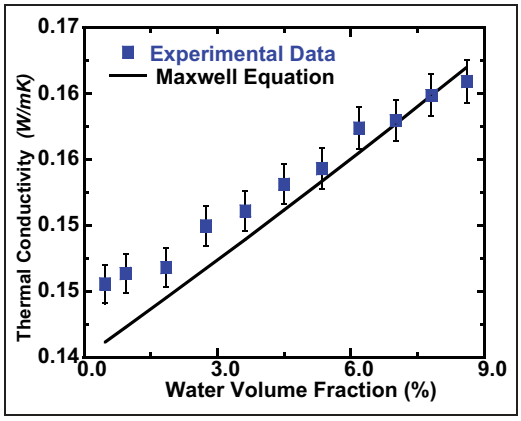

Figure 4. Thermal conductivity of water/PAO nanoemulsion fluids versus water volume fraction. The prediction from the Maxwell equation is shown for comparison.

determine the nanodroplet geometry by fitting the SANS data especially for scattering q less than 0.1 Å region, and the fitting curves are shown in Figure 3.[35,36,38,50]

Generally, the scattering intensity is given by the two contributions in the Guinier–Porod model

$$I(Q) = \frac{G_2}{Q^{S_2}} \exp\left(\frac{-Q^2 R_{g2}^2}{3 - s_2}\right) \quad \text{for } Q \le Q_2$$
$$I(Q) = \frac{G_1}{Q^{S_1}} \exp\left(\frac{-Q^2 R_{g1}^2}{3 - s_1}\right) \quad \text{for } Q_2 \le Q \le Q_1 \qquad (5)$$
$$I(Q) = \frac{D}{Q^d} \quad \text{for } Q \ge Q_1$$

Here $3 - s_1$ and $3 - s_2$ are the dimensionality parameters, and R_{g1} and R_{g2} are the radii of gyration for the short and overall size of the scattering object. This generalized Guinier–Porod model can be used to analyze SANS patterns for nonspherical objects. In general, for scattering objects with spherical symmetry, $s_1 = s_2 = 0$, and for cylindrical objects, $s_2 = 0$ and $s_1 = 1$. For lamellae with equal width and length, one has $s_2 = 0$ and $s_1 = 2$.

Based on the fitting curves using the 3-region Guinier–Porod model, there are two dimensionality parameters s_1 and s_2, and R_{g2} and R_{g1} are the radii of gyration for the short and overall sizes of the scattering object. The fitted curves give $s_2 = 0.22$, $s_1 = 1.4$ and $R_{g2} = 121$ Å, $R_{g1} = 4.6$ Å for 10.3% volume fraction sample. For 7.8% volume fraction one, $s_2 = 0.18$, $s_1 = 0.97$ and $R_{g2} = 47.4$ Å, $R_{g1} = 5.2$ Å. The dimensionality parameters suggest that those nanodroplets have a cylinder-like shape. So, the SANS data suggest there is an inner structure variation with water loading inside water/PAO nanoemulsion fluids. It is also noteworthy that $s_2 = 0.04$ and $s_1 = 0.25$ is calculated for the 4.5% volume fraction one which can be approximated to $s_2 \approx 0$ and $s_1 \approx 0$ which agree well with the spherical shape using hard-sphere model fitting. Note that for cylindrical droplets, $R_{g2}^2 = L^2/12 + R^2/2$, where L is the cylinder length and R is its radius and $R_{g1}^2 = R^2/2$.

Thermal conductivity characterization

Figure 4 shows the thermal conductivity enhancement in water/PAO nanoemulsion fluids as a function of the loading of water from 0.47% to 8.6% volume fraction at room temperature using the 3ω method we mentioned earlier. In this and other figures, statistical error bars correspond to 1 standard deviation. Pure PAO is used for calibration and its measured value $\kappa_{PAO} = 0.143$ W/m K agrees well with the literature value.

It can be seen that the thermal conductivity increases linearly with water volume fraction. A maximum increase of 16% is observed at a water volume concentration equals 8.6% volume fraction. The observed enhancement in thermal conductivity agrees well with that predicted by the classical Maxwell equation with the assumption of spherical droplets. The Maxwell equation for suspensions of well-dispersed, noninteracting spherical particles[51,52] reads

$$\kappa_{maxwell} = \frac{\kappa_P + 2\kappa_0 + 2\phi(\kappa_P - \kappa_0)}{\kappa_P + 2\kappa_0 - \phi(\kappa_P - \kappa_0)} \times \kappa_0 \qquad (6)$$

where κ_0 is the thermal conductivity of the base fluid, κ_p is the thermal conductivity of the particles, and ϕ is the particle volumetric fraction. Equation (6) predicts that the thermal conductivity enhancement increases approximately linearly with the particle volumetric fraction for dilute nanofluids or nanoemulsion fluids (e.g. $\phi < 10\%$), if $\kappa_p > \kappa_0$ and no change in particle shape.

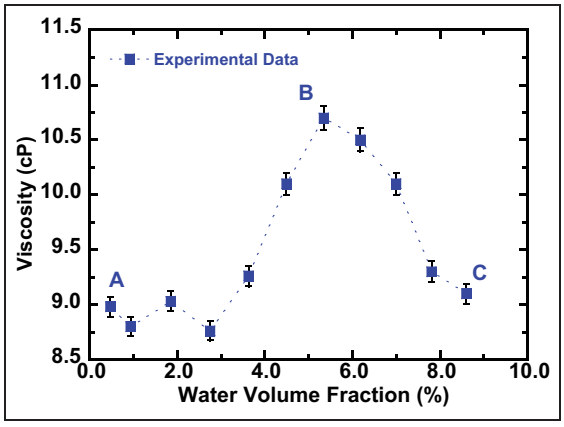

Figure 5. Dynamic viscosity of water/PAO nanoemulsion fluids versus water volume fraction.

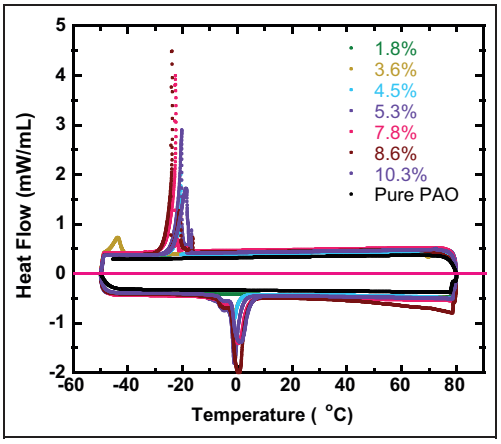

Figure 6. DSC cyclic curves of water/PAO nanoemulsion fluids for different water loadings. Exothermal peaks are observed at −20 °C, corresponding to the freezing of water nanodroplets, while endothermal peaks are observed at 0 °C, corresponding to the melting of water nanodroplets.

Viscosity characterization

The dynamic viscosity of water/PAO nanoemulsion fluids was measured at room temperature and the viscosity dependence upon the water volumetric concentration is shown in Figure 5. The calibration is carried out using the pure PAO and its dynamic viscosity is found to be 7.3 cP which compares very well with the literature value. The test samples exhibit a shear-independent characteristic of Newtonian fluids for the spindle rotational speed from 10 to 30 r/min.

One interesting thing can be seen in Figure 5 that the viscosity first increases with water concentration, reaches a maximum at 5.3% volume fraction, and then decreases. This trend is different from the thermal conductivity shown in Figure 4, and the maximum viscosity can be attributed to the attraction force between droplets within the nanoemulsion fluids. As the amount of water is increased, the surfactant molecules become hydrated while releasing their counterions into water. The exchange of surfactants molecules and counterions between the droplets could make themselves charged oppositely. The interdroplet attraction increases with water concentration until the hydration process is complete. This leads to a maximum viscosity in water/PAO nanoemulsion fluids. It also coincides with the nonlinear inner structure change with increasing water concentration as seen in Figure 3.

Heat capacity

Meanwhile, another important liquid–solid phase change property, the heat capacity of water/PAO nanoemulsion fluids, has also been investigated and shown in Figure 6. Theoretically, the heat capacity can be enhanced through two different mechanisms: one is due to the high specific heat of the dispersed phase; the other is due to the latent heat of the dispersed phase-changeable nanodroplets.[24,41,53–55] The latter one, that is, use of phase-changeable nanodroplets, is much more efficient for the heat capacity enhancement. In water/PAO nanoemulsion fluids, the fluid's heat capacity can be increased by the high specific heat of water (i.e. $C_{water} = 4.2\,\mathrm{J/g\ C}$, $C_{PAO} = 1.88\,\mathrm{J/g\ C}$) or the latent heat of water ($\Delta H = 334\,\mathrm{J/g}$), depending on the operating temperature of the fluids.

When water nanodroplets do not undergo solid–liquid phase change, the specific heat of the water/PAO nanoemulsion fluids follows the simple mixing rule

$$C_{nanoemulsion} = (1 - \Phi)C_{oil} + \Phi C_{water} \tag{7}$$

where Φ represents the concentration of the "water" phase. The specific heat of the pure PAO and water/PAO nanoemulsion fluids are measured using a Differential Scanning Calorimetry (DSC). Besides the observed enhancement of heat capacity with adding water to the base PAO fluid, the impact of phase-changeable water nanodroplets on the fluid properties is obvious. Thus, the effective specific heat of the fluids is calculated using the following equation

$$C_{nanoemulsion} = \frac{C_{base\_fluid} + \phi H_{f,droplet}}{\Delta T} \tag{8}$$

where ϕ is the volume fraction of the phase-changeable nanodroplets, $H_{f,droplet}$ is the latent heat of the phase-changeable nanodroplets per unit volume, and ΔT is the temperature difference between the heat transfer surface and the bulk fluid.

DSC cyclic curves of water/PAO nanoemulsion fluids under different water loadings are shown in Figure 6. During the heating and cooling cycles, water nanodroplets undergo a melting–freezing transition in

Table 1. Specific heat of water/PAO nanoemulsion fluids with its supercooling temperature.

Water % fractions	Heat of fusion (J/g)	Peak T (°C)
10.3	28.97	−18.88
8.6	34.17	−23.97
7.8	31.27	−22.74
5.3	26.72	−20.32
4.5	9.808	−20.63
3.6	2.48	−45
1.8	2.18	0

PAO: polyalphaolefin.

the nanoemulsion fluids. The observed melting–freezing hysteresis (i.e. supercooling) varies from 20 °C to 45 °C, depending on the size of the droplets and the structure of the microemulsion, while most of the peaks occur at about −20 °C). The hysteresis in the melting–freezing cycle may be due to the interfacial energy change inside nanoemulsion fluids. On the other hand, the presence of a single freezing peak in Figure 6 indicates a correspondence of the structural change with increasing water concentration (or water-to-surfactant molar ratio) as observed in our previous SANS measurement result. There is no obvious melting–freezing peak for water concentrations less than 4.5%, while the exothermic crystallization peak starts at around −20 °C when water concentration is higher or equal to 4.5%. When the water concentration is increased further to above 8.6%, the freezing peak shifts to effect lower supercooling and peak values.

To quantify the specific heat of each sample, the result is also calculated and summarized here in Table 1. It can be seen here that the specific heat sharply increases from 9.8 to 26.72 J/g when the water concentration is increased from 4.5% to 5.3%. It gradually increases with higher water concentration and decreases again when the water concentration is higher than 8.6%, while the freezing peak temperature is decreased. All these happen to coincide with the structure transition from spherical to cylinder shape with increasing water concentrations as observed from SANS measurement.

Assuming $\Delta T = 20$ °C, the effective volumetric specific heat can be increased by up to 80% for the nanoemulsion fluid containing 8.6% water nanodroplets when the water nanodroplets undergo phase transition. The use of phase-changeable nanodroplets is expected to provide a way to simultaneously increase the effective specific heat and thermal conductivity of conventional heat transfer fluids. Meanwhile, the heat of fusion H_f of pure water is 334 J/g, an outstanding value among phase-changing materials. The calculated H_f values of water/PAO nanoemulsions for different water loading from 5.3 to 8.6 volumetric percent are 17.7 and 28.724 J/g, respectively, in agreement with the measured results shown in Table 1, which are 26.72 and 34.17 J/g, respectively. The volumetric heat capacity of water is about 4.18 J/mL K, and is over two times the heat capacity of PAO (1.74 J/mL K).[26] For a temperature increase from −20 °C to 0 °C, 1-mL PAO absorbs 37.6-J heat. For the nanoemulsion containing 8.6% water nanodroplets, the melting of ice nanoparticle absorbs 34-J heat, which means that upon melting the ice nanoparticles in the nanoemulsion, the heat capacity of PAO has increased up by about 76%. Together with the enhancement in heat capacity caused only by the addition of water without phase change, totally a maximum heat capacity increase of 88% is obtained in the 8.6% water/PAO nanoemulsion fluids.

Conclusion

In summary, thermophysical properties such as the thermal conductivity, the viscosity, and the specific heat have been investigated along with the inner structure of water/PAO nanoemulsion fluids. The thermal conductivity increase is rather moderate in these fluids, for example, a 16% increase for 8.6% volume fraction sample, which agrees well with the classical colloidal theory. The dynamic viscosity exhibits a maximum value of 10.7 cP at a water volume concentration around 5.3% which coincides with the variation of the nanosrtructure inside at different water concentrations. The effective specific heat can be greatly enhanced when the water nanodroplets undergo phase change: it can be increased up to 90%. Future research will aim at correlating the phase change process with inner structure change, and/or nucleation mechanism will be particularly beneficial, as such phenomena are typically not well understood in complex colloidal systems. Additionally, to enhance the thermophysical properties further, future investigations could focus on a systematical study and comparison of different nanoemulsion systems.

Authors note

The identification of commercial products does not imply endorsement by the National Institute of Standards and Technology nor does it imply that these are the best for the purpose.

Declaration of conflicting interests

The authors declare that there is no conflict of interests regarding the publication of this article.

Funding

This study is financially supported by National Science Foundation (CBET-0730963). The SANS measurements performed at the NIST-CNR are supported in part by the National Science Foundation under agreement no. DMR-0944772.

References

1. Agostini B, Fabbri M, Park JE, et al. State of the art of high heat flux cooling technologies. *Heat Tran Eng* 2007; 28: 258–281.
2. Dewan A, Mahanta P, Raju KS, et al. Review of passive heat transfer augmentation techniques. *Proc IME J Power Energ* 2004; 218: 509–527.
3. Ahn HS and Kim MH. A review on critical heat flux enhancement with nanofluids and surface modification. *J Heat Tran Trans: ASME* 2012; 134: 024001.
4. Arik M and Bar-Cohen A. Pool boiling of perfluorocarbon mixtures on silicon surfaces. *Int J Heat Mass Tran* 2010; 53: 5596–5604.
5. Barber J, Brutin D and Tadrist L. A review on boiling heat transfer enhancement with nanofluids. *Nanoscale Res Lett* 2011; 6: 280.
6. Farid MM, Khudhair AM, Razack SAK, et al. A review on phase change energy storage: materials and applications. *Energ Convers Manage* 2004; 45: 1597–1615.
7. Inaba H. New challenge in advanced thermal energy transportation using functionally thermal fluids. *Int J Therm Sci* 2000; 39: 991–1003.
8. Thome JR. The new frontier in heat transfer: microscale and nanoscale technologies. *Heat Tran Eng* 2006; 27: 1–3.
9. Wasekar VM and Manglik RM. A review of enhanced heat transfer in nucleate pool boiling of aqueous surfactant and polymeric solutions. *J Enhanc Heat Tran* 1999; 6: 135–150.
10. Zimparov V. Energy conservation through heat transfer enhancement techniques. *Int J Energ Res* 2002; 26: 675–696.
11. El-Genk MS and Parker JL. Nucleate boiling of FC-72 and HFE-7100 on porous graphite at different orientations and liquid subcooling. *Energ Convers Manage* 2008; 49: 733–750.
12. Zhang H, Mudawar I and Hasan MM. Assessment of dimensionless CHF correlations for subcooled flow boiling in microgravity and earth gravity. *Int J Heat Mass Tran* 2007; 50: 4568–4580.
13. Buongiorno J, Hu LW, Kim SJ, et al. Nanofluids for enhanced economics and safety of nuclear reactors: an evaluation of the potential features, issues, and research gaps. *Nucl Technol* 2008; 162: 80–91.
14. Coursey JS and Kim J. Nanofluid boiling: the effect of surface wettability. *Int J Heat Fluid Flow* 2008; 29: 1577–1585.
15. Milanova D and Kumar R. Heat transfer behavior of silica nanoparticles experiment in pool boiling. *J Heat Trans: T ASME* 2008; 130: 042401.
16. Wong KV and De Leon O. Applications of nanofluids: current and future. *Adv Mech Eng* 2010; 2010: 1–11.
17. Xu J and Zhang Y. Analysis of heat transfer during liquid-vapor pulsating flow in a U-shaped miniature channel. *J Enhanc Heat Tran* 2009; 16: 367–385.
18. Xu J, Zhang Y and Ma H. Effect of internal wick structure on liquid-vapor oscillatory flow and heat transfer in an oscillating heat pipe. *J Heat Tran Trans ASME* 2009; 131: 121012.
19. Xu JJ, Wu CW and Yang B. Thermal- and phase-change characteristics of self-assembled ethanol/polyalphaolefin nanoemulsion fluids. *J Thermophys Heat Tran* 2010; 24: 208–211.
20. Xu J, Yang B and Hammouda B. Thermal conductivity and viscosity of self-assembled alcohol/polyalphaolefin nanoemulsion fluids. *Nanoscale Res Lett* 2011; 6: 274.
21. Xu J and Yang B. Nanostructured phase-changeable heat transfer fluids. *Nanotechnol Rev* 2013; 2(3): 289–306. DOI: 10.1515/ntrev-2012-0041.
22. Xu J, Hammouda B and Yang B. Thermophysical properties and pool boiling characteristics of water in polyalphaolefin nanoemulsion fluids. In: *Proceedings of ASME micro/nanoscale heat & mass transfer international conference*, Atlanta, GA, 3–6 March 2012, pp. 321–325. New York: ASME.
23. Yang B. Thermal conductivity equations based on Brownian motion in suspensions of nanoparticles (nanofluids). *J Heat Tran Trans ASME* 2008; 130: 042408.
24. Han ZH and Yang B. Thermophysical characteristics of water-in-FC72 nanoemulsion fluids. *Appl Phys Lett* 2008; 92: 013118.
25. Yang B and Han ZH. Thermal conductivity enhancement in water-in-FC72 nanoemulsion fluids. *Appl Phys Lett* 2006; 88: 261914.
26. *Synfluid PAO databook*. The Woodlands, TX: Chevron Phillips Chemical LP, 2002.
27. Han ZH, Yang B, Qi Y, et al. Synthesis of low-melting-point metallic nanoparticles with an ultrasonic nanoemulsion method. *Ultrasonics* 2011; 51: 485–488.
28. Shaikh S, Lafdi K and Ponnappan R. Thermal conductivity improvement in carbon nanoparticle doped PAO oil: an experimental study. *J Appl Phys* 2007; 101: 064302.
29. Das SK, Putra N, Thiesen P, et al. Temperature dependence of thermal conductivity enhancement for nanofluids. *J Heat Tran Trans ASME* 2003; 125: 567–574.
30. Eastman JA, Phillpot SR, Choi SUS, et al. Thermal transport in nanofluids. *Ann Rev Mater Res* 2004; 34: 219–246.
31. Jeong YH, Chang WJ and Chang SH. Wettability of heated surfaces under pool boiling using surfactant solutions and nano-fluids. *Int J Heat Mass Tran* 2008; 51: 3025–3031.
32. Wen D. Mechanisms of thermal nanofluids on enhanced critical heat flux (CHF). *Int J Heat Mass Tran* 2008; 51: 4958–4965.
33. Chen SH. Small-angle neutron-scattering studies of the structure and interaction in micellar and microemulsion systems. *Annu Rev Phys Chem* 1986; 37: 351–399.
34. Gradzielski M and Langevin D. Small-angle neutron scattering experiments on microemulsion droplets: relation to the bending elasticity of the amphiphilic film. *J Mol Struct* 1996; 383: 145–156.
35. Hammouda B, Krueger S and Glinka CJ. Small-angle neutron-scattering at the National Institute of Standards and Technology. *J Res Natl Inst Stan* 1993; 98: 31–46.
36. Hammouda B. SANS from polymers: review of the recent literature. *Polym Rev* 2010; 50: 14–39.

37. Howe AM, Toprakcioglu C, Dore JC, et al. Small-angle neutron-scattering studies of microemulsions stabilized by aerosol-OT. Part 3. The effect of additives on phase-stability and droplet structure. *J Chem Soc Faraday Trans 1* 1986; 82: 2411–2422.
38. Marszalek J, Pojman JA and Page KA. Neutron scattering study of the structural change induced by photopolymerization of AOT/D_2O/dodecyl acrylate inverse microemulsions. *Langmuir* 2008; 24: 13694–13700.
39. Nagao M, Seto H, Shibayama M, et al. Small-angle neutron scattering study of droplet density dependence of the water-in-oil droplet structure in a ternary microemulsion. *J Appl Crystallogr* 2003; 36: 602–606.
40. Cahill DG. Thermal-conductivity measurement from 30-K to 750-K: the 3-Omega method. *Rev Sci Instrum* 1990; 61: 802–808.
41. Han ZH, Cao FY and Yang B. Synthesis and thermal characterization of phase-changeable indium/polyalphaolefin nanofluids. *Appl Phys Lett* 2008; 92: 243104.
42. Hasselman DPH and Johnson LF. Effective thermal-conductivity of composites with interfacial thermal barrier resistance. *J Compos Mater* 1987; 21: 508–515.
43. Han ZH, Yang B, Kim SH, et al. Application of hybrid sphere/carbon nanotube particles in nanofluids. *Nanotechnology* 2007; 18: 105701.
44. Yang B, Liu WL, Liu JL, et al. Measurements of anisotropic thermoelectric properties in superlattices. *Appl Phys Lett* 2002; 81: 3588–3590.
45. Yang B and Han ZH. Temperature-dependent thermal conductivity of nanorod-based nanofluids. *Appl Phys Lett* 2006; 89: 083111.
46. Dames C, Chen S, Harris CT, et al. A hot-wire probe for thermal measurements of nanowires and nanotubes inside a transmission electron microscope. *Rev Sci Instrum* 2007; 78: 104903.
47. Batra U, Russel WB and Huang JS. Viscosity anomaly and charge fluctuations in dilute AOT microemulsions with $X < 20$. *Langmuir* 1999; 15: 3718–3725.
48. Bergenholtz J, Romagnoli AA and Wagner NJ. Viscosity, microstructure, and interparticle potential of AOT/H_2O/*n*-decane inverse microemulsions. *Langmuir* 1995; 11: 1559–1570.
49. Chiesa M, Garg J, Kang YT, et al. Thermal conductivity and viscosity of water-in-oil nanoemulsions. *Colloid Surface A Physicochem Eng Aspect* 2008; 326: 67–72.
50. Hammouda B. A new Guinier-Porod model. *J Appl Crystallogr* 2010; 43: 716–719.
51. Maxwell JC. *A treatise on electricity and magnetism*. Cambridge: Oxford University Press, 1904.
52. Buongiorno J, Venerus DC, Prabhat N, et al. A benchmark study on the thermal conductivity of nanofluids. *J Appl Phys* 2009; 106: 094312.
53. Moulik SP, Das ML, Bhattacharya PK, et al. Thermodynamics of microemulsion formation. 1. Enthalpy of solution of water in binary (Triton-X 100 + Butanol) and ternary (Heptane + Triton-X 100 + Butanol) mixtures and heat-capacity of the resulting systems. *Langmuir* 1992; 8: 2135–2139.
54. Mulligan JC, Colvin DP and Bryant YG. Microencapsulated phase-change material suspensions for heat transfer in spacecraft thermal systems. *J Spacecraft Rockets* 1996; 33: 278–284.
55. Ray S, Bisal SR and Moulik SP. Thermodynamics of microemulsion formation. 2. Enthalpy of solution of water in binary-mixtures of aerosol-OT and heptane and heat-capacity of the resulting systems. *Langmuir* 1994; 10: 2507–2510.

Appendix 1

Notation

C	heat capacity ($J/m^3 K$)
h	convective heat transfer coefficient ($W/m^2 K$)
H	heat of vaporization (J/m^3)
P	pressure (N/m^2)
q	heat flux (W/m^2)
T	temperature (°C)
V	volume (m^3)
μ	fluid viscosity ($N\ s/m^2$)
u	velocity (m/s)
ρ	mass density (kg/m^3)
ϕ	volume fraction (%)